



**HAL**  
open science

## Enhanced Ultraviolet Stability of Air-Processed Polymer Solar Cells by Al Doping of the ZnO Interlayer

Mario Prosa, Marta Tessarolo, Margherita Bolognesi, Olivier Margeat, Desta Gedefaw, Meriem Gaceur, Christine Videlot-Ackermann, Mats R. Andersson, Michele Muccini, Mirko Seri, et al.

### ► To cite this version:

Mario Prosa, Marta Tessarolo, Margherita Bolognesi, Olivier Margeat, Desta Gedefaw, et al.. Enhanced Ultraviolet Stability of Air-Processed Polymer Solar Cells by Al Doping of the ZnO Interlayer. ACS Applied Materials & Interfaces, 2016, 8 (3), pp.1635-1643. 10.1021/acsami.5b08255 . hal-01453099

**HAL Id: hal-01453099**

**<https://hal.science/hal-01453099>**

Submitted on 1 Feb 2024

**HAL** is a multi-disciplinary open access archive for the deposit and dissemination of scientific research documents, whether they are published or not. The documents may come from teaching and research institutions in France or abroad, or from public or private research centers.

L'archive ouverte pluridisciplinaire **HAL**, est destinée au dépôt et à la diffusion de documents scientifiques de niveau recherche, publiés ou non, émanant des établissements d'enseignement et de recherche français ou étrangers, des laboratoires publics ou privés.

# Enhanced Ultraviolet Stability of Air-Processed Polymer Solar Cells by Al Doping of the ZnO Interlayer

Mario Prosa,<sup>†</sup> Marta Tassarolo,<sup>†</sup> Margherita Bolognesi,<sup>‡</sup> Olivier Margeat,<sup>§</sup> Desta Gedefaw,<sup>||,⊥</sup> Meriem Gaceur,<sup>§</sup> Christine Videlot-Ackermann,<sup>§</sup> Mats R. Andersson,<sup>||,⊥</sup> Michele Muccini,<sup>†</sup> Mirko Seri,<sup>\*,#</sup> and Jörg Ackermann<sup>\*,§</sup>

<sup>†</sup>Consiglio Nazionale delle Ricerche (CNR) – Istituto per lo Studio dei Materiali Nanostrutturati (ISMN), Via P. Gobetti, 101, 40129 Bologna, Italy

<sup>‡</sup>Laboratory MIST E-R, Via P. Gobetti, 101, 40129 Bologna, Italy

<sup>§</sup>Aix-Marseille Université, CNRS, CINaM UMR 7325, 13288 Marseille, France

<sup>||</sup>Department of Chemistry and Chemical Engineering, Polymer Technology, Chalmers University of Technology, Goteborg SE-412 96, Sweden

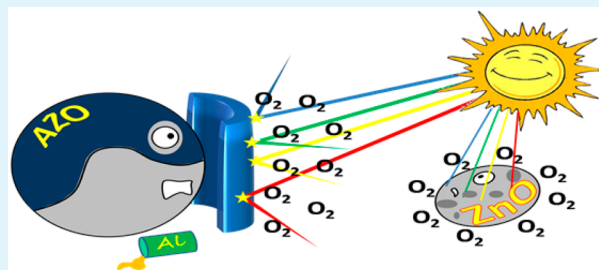
<sup>⊥</sup>Ian Wark Research Institute, Future Industries Institute, University of South Australia, Mawson Lakes, South Australia 5095, Australia

<sup>#</sup>Consiglio Nazionale delle Ricerche (CNR) – Istituto per la Sintesi Organica e la Fotoreattività (ISOF), Via P. Gobetti, 101, 40129 Bologna, Italy

## Supporting Information

**ABSTRACT:** Photostability of organic photovoltaic devices represents a key requirement for the commercialization of this technology. In this field, ZnO is one of the most attractive materials employed as an electron transport layer, and the investigation of its photostability is of particular interest. Indeed, oxygen is known to chemisorb on ZnO and can be released upon UV illumination. Therefore, a deep analysis of the UV/oxygen effects on working devices is relevant for the industrial production where the coating processes take place in air and oxygen/ZnO contact cannot be avoided. Here we investigate the light-soaking stability of inverted organic solar cells in which four different solution-processed ZnO-based nanoparticles were used as electron transport layers: (i) pristine ZnO, (ii) 0.03 at %, (iii) 0.37 at %, and (iv) 0.8 at % aluminum-doped AZO nanoparticles. The degradation of solar cells under prolonged illumination (40 h under 1 sun), in which the ZnO/AZO layers were processed in air or inert atmosphere, is studied. We demonstrate that the presence of oxygen during the ZnO/AZO processing is crucial for the photostability of the resulting solar cell. While devices based on undoped ZnO were particularly affected by degradation, we found that using AZO nanoparticles the losses in performance, due to the presence of oxygen, were partially or totally prevented depending on the Al doping level.

**KEYWORDS:** polymer solar cells, aluminum-doped ZnO, photostability, ZnO nanoparticles, degradation, oxygen chemisorption, interlayer



## INTRODUCTION

In the last decades, scientific interest gradually converged on organic photovoltaics (OPVs) as a promising energy technology in the field of renewable sources. The potential of low cost at large production in conjunction with lightweight and flexible devices promoted OPVs as a valid alternative to inorganic photovoltaics.<sup>1,2</sup> In sight of this, research focused on polymer solar cells (PSCs) in which a solution-processed photoactive layer made by a mixture of a donor polymer and a fullerene-based acceptor (bulk heterojunction, BHJ) is sandwiched between two electrodes, a cathode and an anode.<sup>3</sup> The BHJ concept should ensure an efficient exciton separation after light absorption and bicontinuous paths for

charges to be collected at their respective electrodes. In addition, selective interlayers, i.e., buffer layers, are introduced between the electrodes and the active layer promoting ohmic contact and improving the charge collection selectivity.<sup>4</sup>

Over the years, the optimization of all these layers led to clear improvements for PSCs in terms of power conversion efficiency (PCE).<sup>5</sup> Moreover, the development of multijunction architectures pushed the performance of OPVs up to 11.8%.<sup>6</sup> However, for the commercialization of this technology, one

Received: September 3, 2015

Accepted: December 23, 2015

Published: January 11, 2016

challenging problem is still represented by the reliability or lifetime of modules.<sup>7</sup> Organic materials are very sensitive to ambient agents including humidity and oxygen. In addition, working devices are subjected to solar heating and light which could cause thermally induced and photoinduced degradation, respectively, of the materials as well as interfaces.<sup>8</sup> Some of these issues can be prevented by encapsulating the device after fabrication, thus avoiding oxygen and water diffusion inside the solar cell. Moreover, to counter the issue of short-term degradation, the concept of “inverted” geometry devices has been introduced.<sup>9</sup> This type of configuration is proven to be more stable than the conventional one because no low work function metal electrode is exposed to ambient, and therefore deterioration of the cell performance due to oxidation is prevented.<sup>10</sup> Furthermore, BHJ active layers have been demonstrated to undergo morphological changes under thermal stress, affecting the device performance. Since the internal/adjacent interfaces strongly influence the morphological behavior of the BHJ layer during thermal stress, the use of an inverted structure has been proved to often improve the thermal stability of the resulting devices.<sup>11–14</sup>

In order to optimize the charge collection at the electrodes in inverted structures, air-stable, high work function materials, e.g., PEDOT:PSS or MoO<sub>3</sub>, are typically used as an interlayer at the top anode as a hole-transporting layer (HTL), while low work function materials like PFN, PEIE, TiO<sub>x</sub>, or ZnO are deposited on ITO (cathode) acting as an electron transport layer (ETL).<sup>4</sup>

Among ETLs, ZnO is very attractive for its high electron conductivity, low work function, good optical transmittance, non toxicity, and low cost.<sup>15–19</sup> In addition, ZnO can be synthesized in the form of nanoparticles (ZnO NPs) which can be deposited from solution generating thin films with high conductivity without the need of strong thermal treatments.<sup>16,18–20</sup>

Despite that ZnO shows a variety of suitable properties for photovoltaic applications, one limitation is that its conductivity is negatively affected by chemisorbed oxygen (O<sub>2</sub>).<sup>21</sup> O<sub>2</sub> molecules are able to capture electrons from the conduction band of ZnO, creating near the surface a depletion region with high resistivity.<sup>22</sup> This process is physically reversible, and if ZnO is irradiated with ultraviolet light, oxygen molecules can be released from the ZnO layer leading to an improvement of the ZnO conductivity.<sup>23,24</sup>

Although light irradiation could restore the conductivity of ZnO, prolonged illumination could induce irreversible degradation.<sup>25–28</sup> Indeed, UV light soaking in the presence of oxygen triggers the formation of “chemical defects”, which reduce the n-type behavior of the ZnO. These are likely p-type defects of the lattice structure that induce an increase of the ZnO work function.

As a consequence, the presence of oxygen during ZnO film processing could represent an issue for the photostability of solar cells. In addition, since the adsorption of oxygen is a surface-related phenomenon, structures with a high surface-to-volume ratio, as in the case of films of ZnO NPs, might be particularly sensitive to light exposure if processed in air.<sup>29</sup> In this context, a deeper investigation on the role of light soaking on solar cells containing a layer of air-processed ZnO NPs is of particular interest.

Despite the above-mentioned suitability of ZnO for photovoltaic applications, the use of undoped ZnO for large-scale production of optoelectronic devices could be challenging in terms of processing. Indeed, in industrial fabrication, relatively

thick layers in the order of 100 nm are preferred to ensure complete substrate coverage and avoid the risk of defects. Since the conductance of such a thick layer of ZnO would not be sufficient to ensure a good photovoltaic performance of the relative devices,<sup>30</sup> ZnO is usually doped with small amounts of metal ions, such as Al, Ga, etc. Among them, aluminum-doped ZnO (AZO) is one of the most studied materials for OPV applications.<sup>31</sup> As AZO can be produced in the form of nanoparticles,<sup>32</sup> it has the same advantages of undoped ZnO NPs in terms of layer processing, while having a conductivity which can be three orders of magnitude higher.<sup>33,34</sup> AZO is therefore introduced to facilitate the use of ZnO-based materials in industrial processes like roll-to-roll coating.

Roll-to-roll industrial coating processes mostly take place in ambient conditions, and the effect of air as well as light soaking of undoped ZnO is known to be detrimental. Therefore, it is crucial to understand the effects of prolonged illumination on solar cells based on air-processed AZO films.

In this work we present a study on the light soaking degradation of inverted polymer solar cells using different formulations of ZnO-based NPs as ETLs: (i) pristine and (ii) 0.03 at %, (iii) 0.37 at %, and (iv) 0.8 at % aluminum-doped. We investigated and compared the degradation under prolonged illumination (40 h under 1 sun) of the resulting solar cells in which the ZnO/AZO layers are processed in air or an inert atmosphere. We found that all the devices showed similar stability when the ZnO/AZO layers are processed in an inert atmosphere. Importantly, in the case of air-processed layers, the stability of the solar cells was dependent on the aluminum doping level in the ZnO NPs. We demonstrate that the presence of oxygen during the ZnO/AZO processing is crucial for the photostability of the resulting solar cell. In particular, air-processed devices based on undoped ZnO (ETL) are particularly affected by degradation, while using AZO NPs, the loss of performance ascribed to ZnO/oxygen interaction can be partially or totally prevented depending on the Al doping level.

## ■ EXPERIMENTAL SECTION

**AZO Nanoparticle Synthesis and Characterization.** Details on the synthesis of AZO NPs containing doping levels from 0% to 0.8% of Al (atomic percentages) are given elsewhere.<sup>35</sup> AZO NPs with 0%, 0.03%, 0.37%, and 0.8% Al doping level are named ZnO, AZO<sub>0.03</sub>, AZO<sub>0.37</sub>, and AZO<sub>0.8</sub>, respectively. In a typical synthesis of AZO<sub>0.03</sub>, zinc acetate (0.779 g, 4.24 mmol), aluminum isopropylate (0.009 g, 0.04 mmol), and 0.25 mL of distilled water were added into a flask containing 42 mL of anhydrous ethanol. The solution was heated to 80 °C with magnetic stirring during 30 min. A solution of 0.442 g of potassium hydroxide in 23 mL of ethanol was added dropwise to the flask. After adding the base, the solution was stirred for 16 h at 80 °C. The reaction mixture was then allowed to cool, and the AZO NPs were separated from the reaction mixture by centrifugation (7800 rpm for 30 min) and then dispersed in alcohol-based solvents. The morphology of the AZO NPs bearing different Al doping were characterized by HR-TEM. Figure S1 shows a representative TEM analysis of AZO<sub>0.03</sub> NPs. We found that all AZO NPs show a narrow size distribution and average diameter of 10 nm independently from the doping level, making these NPs highly suitable for solution processing of AZO interfacial layers. In order to process thin films, isopropanol solutions containing AZO NPs of different concentrations were prepared. Importantly, ethanalamine (EA) was used to obtain cluster-free solution as demonstrated recently.<sup>19</sup> The aggregate size of the AZO NPs within the solution was controlled by dynamic light scattering (DLS) analysis revealing that the EA treatment generates highly dispersed stable AZO solution regardless of the doping level.

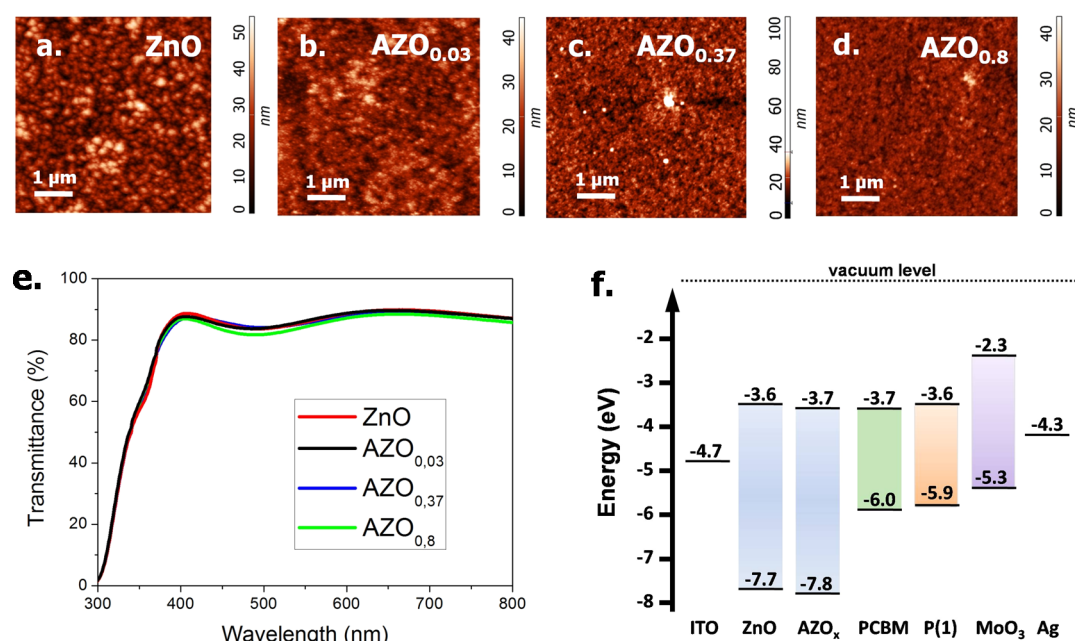


**Figure 1.** Atomic force microscopy (AFM) images ( $5 \mu\text{m} \times 5 \mu\text{m}$ ) recorded in tapping mode of ZnO (a), AZO<sub>0.03</sub> (b), AZO<sub>0.37</sub> (c), and AZO<sub>0.8</sub> (d) deposited on glass/ITO substrates. Their surface roughness (RMS) is 8, 6, 4, and 4 nm, respectively. Transmittance spectra (e) of ZnO (red), AZO<sub>0.03</sub> (black), AZO<sub>0.37</sub> (blue), and AZO<sub>0.8</sub> (green) films deposited on glass/ITO substrates. Energy level diagram of the materials employed in the solar cells (f).

**Solar Cell Fabrication and Characterization.** All materials, PC<sub>61</sub>BM ([6,6]-phenyl-C61-butyric acid methyl ester, American Dye Source), 1,2-dichlorobenzene (ODCB, Sigma-Aldrich), and 1,8-diiodooctane (DIO, Sigma-Aldrich) were purchased from commercial sources and used without further purification. Patterned ITO-coated glasses (thickness = 150 nm,  $R_s \sim 10 \Omega \text{sq}^{-1}$ , ITO roughness RMS < 1 nm) were cleaned in sequential sonicating baths (for 15 min) of acetone and isopropanol. After the final sonication step, substrates were dried with a stream of Ar gas and then placed in an oxygen plasma chamber for 10 min. Next, a thin layer ( $\sim 40$  nm) of ZnO or AZO<sub>x</sub> was spun-cast on the ITO surface in ambient atmosphere or inside a N<sub>2</sub>-filled glovebox (H<sub>2</sub>O and O<sub>2</sub> concentration < 0.1 ppm) and subsequently annealed at 140 °C for 15 min. In the case of air-processed ZnO/AZO<sub>x</sub> films, immediately after the thermal treatment, the samples were transferred in a N<sub>2</sub>-filled glovebox to avoid water adsorption. Note that two (identical) batches of the already known ZnO/AZO<sub>x</sub><sup>35</sup> have been prepared and used to confirm the reproducibility of the synthetic procedure and to validate the impact of their intrinsic properties on the corresponding photovoltaic devices. The active layer blend solutions were formulated inside the glovebox by dissolving the polymer P(1)-PFQ2T-BDT (abbreviated as P(1) in the text) and PC<sub>61</sub>BM (1:1 wt/wt ratio) in anhydrous ODCB:DIO (97:3 v/v) with a total concentration of 30 mg/mL and then stirred overnight at 80 °C. The active layer was prepared inside the glovebox by spinning the blend solution on top of the ITO/ZnO or AZO<sub>x</sub> surface. The wet films were slowly dried resulting in a  $\sim 100$  nm thick layer. To complete the device fabrication, MoO<sub>3</sub> and Ag (10 and 90 nm, respectively) were deposited sequentially without breaking vacuum ( $\sim 1 \times 10^{-6}$  Torr) using a thermal evaporator directly connected to the glovebox. The current–voltage ( $I$ – $V$ ) characteristics of all OPV devices were recorded inside the glovebox by a Keithley 2400 source measure unit under a simulated AM1.5 G illumination of 100 mW/cm<sup>2</sup> (Abet Technologies Sun 2000 Solar Simulator). The light intensity was determined by a calibrated silicon solar cell fitted with a KG5 color glass filter to bring spectral mismatch to unity. The active area of the solar cell was exactly 6 mm<sup>2</sup>. During testing, each cell was carefully masked, by a calibrated mask, to prevent an excess photocurrent generated from the parasitic device regions outside the overlapped electrode area.

**Thin Film Characterization and Device Degradation.** All thin-film characterizations were performed in air. The thickness of the various films was measured by a profilometer (KLA Tencor, P-6). Transmittance UV–vis spectra were recorded on a JASCO V-550 spectrophotometer. The surface morphology of ZnO/AZO layers deposited on top of ITO was studied by atomic force microscopy (AFM) using a Solver Pro (NT-934 MDT) scanning probe microscope in tapping mode. The light soaking test of all solar cells was performed on nonencapsulated devices inside a glovebox under AM1.5G illumination. In a specific test, a colored UV long pass filter at 400 nm was used during light exposure.

## RESULTS AND DISCUSSION

**Characterization of ZnO/AZO<sub>x</sub> Thin Films.** Figure 1 shows the optical and morphological properties and the energy levels of ZnO, AZO<sub>0.03</sub>, AZO<sub>0.37</sub>, and AZO<sub>0.8</sub> films.

The morphology of all the films deposited on ITO is homogeneous, and the surfaces are relatively smooth with a roughness (RMS) of 8, 6, 4, and 4 nm for ZnO, AZO<sub>0.03</sub>, AZO<sub>0.37</sub>, and AZO<sub>0.8</sub>, respectively (Figure 1a–d). All the ZnO-based layers are characterized by similar UV–vis spectra with an optical transmittance higher than 80% over the entire visible range and an absorption peak at 345 nm (Figure 1e). The optical properties, in conjunction with the relatively low surface roughness, make the ZnO-based films compatible for their incorporation in polymer solar cells. Moreover, the energy levels of the valence band and of the conduction band are similar for all ZnO (–7.7 and –3.6 eV, respectively) and AZO<sub>x</sub> (–7.8 and –3.7 eV, respectively) layers,<sup>35</sup> providing well matching contact energetics with the active blend (Figure 1f) thus facilitating the electron extraction process. This makes the films suitable for use as efficient and selective ETLs in BHJ devices. To note, ZnO, AZO<sub>0.03</sub>, AZO<sub>0.37</sub>, and AZO<sub>0.8</sub> are characterized by similar optical, morphological, and energy band positions which do not depend on the aluminum concentration in the NPs.

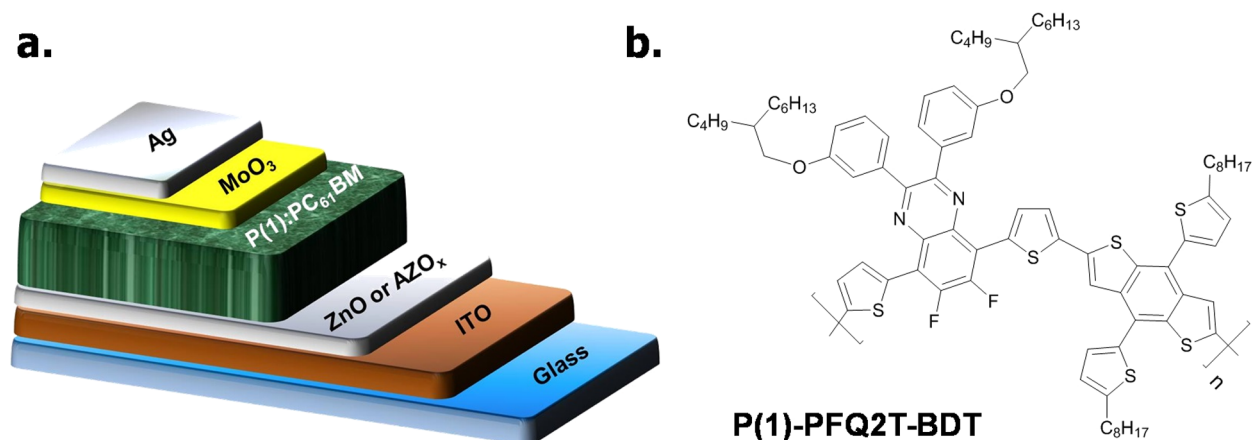


**Figure 2.** Schematic representation of the layers stack of the inverted solar cell (a) and chemical structure of the polymer used as donor material in the active layer (b).

**Table 1.** Photovoltaic Parameters, under Standard Illumination, of Fresh Solar Cells Based on (i) ZnO, (ii) AZO<sub>0.03</sub>, (iii) AZO<sub>0.37</sub>, and (iv) AZO<sub>0.8</sub> ETLs Processed in Air or in Inert Atmosphere, N<sub>2</sub><sup>a</sup>

	ETL	ETL process environment	$J_{sc}$ (mA/cm <sup>2</sup> )	$V_{oc}$ (V)	FF (%)	PCE (%)	$R_s$ ( $\Omega$ cm <sup>2</sup> ) <sup>b</sup>	$R_{sh}$ ( $\Omega$ cm <sup>2</sup> ) <sup>c</sup>
Device A	ZnO	N <sub>2</sub>	8.6 ± 0.3	0.87 ± 0.003	55 ± 2	4.1 ± 0.1	11.5 ± 0.1	670 ± 10
		Air	8.8 ± 0.3	0.87 ± 0.005	55 ± 1	4.2 ± 0.1	10.8 ± 0.1	670 ± 10
Device B	AZO <sub>0.03</sub>	N <sub>2</sub>	8.7 ± 0.1	0.87 ± 0.003	55 ± 1	4.2 ± 0.1	10.8 ± 0.1	680 ± 10
		Air	8.8 ± 0.3	0.87 ± 0.006	54 ± 2	4.1 ± 0.1	11.3 ± 0.1	660 ± 10
Device C	AZO <sub>0.37</sub>	N <sub>2</sub>	8.7 ± 0.3	0.87 ± 0.004	55 ± 2	4.2 ± 0.1	11.0 ± 0.1	690 ± 10
		Air	8.7 ± 0.3	0.87 ± 0.005	55 ± 2	4.2 ± 0.1	11.5 ± 0.1	650 ± 10
Device D	AZO <sub>0.8</sub>	N <sub>2</sub>	8.6 ± 0.2	0.86 ± 0.005	56 ± 1	4.1 ± 0.1	10.5 ± 0.1	690 ± 10
		Air	8.8 ± 0.2	0.86 ± 0.009	54 ± 1	4.1 ± 0.1	10.2 ± 0.1	690 ± 10

<sup>a</sup>All the OPV parameters are averaged over 10 samples, and mean values are reported with their standard deviation. <sup>b</sup> $R_s$  was calculated as the slope of the tangent line of the current density–voltage ( $J$ – $V$ ) curve at  $V > V_{oc}$ . <sup>c</sup> $R_{sh}$  was calculated as the slope of the tangent line of the  $J$ – $V$  curve at  $V = 0$ .

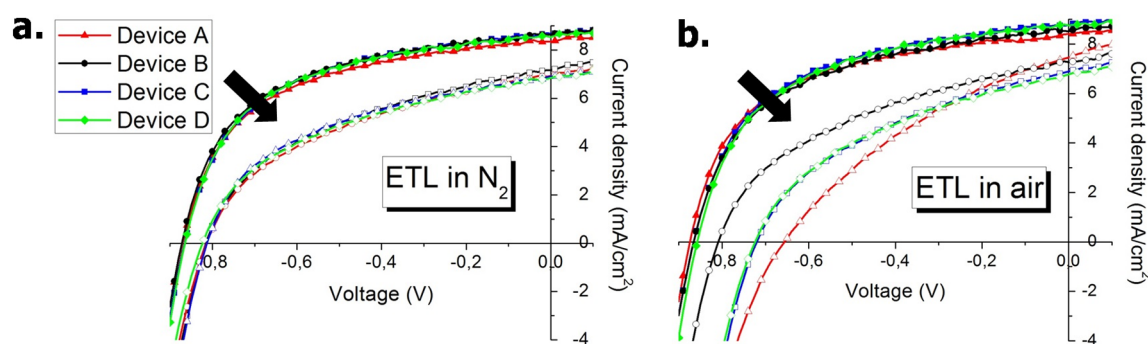


**Figure 3.**  $J$ – $V$  plots of fresh (filled symbols) and degraded under AM1.5G simulated sunlight for 40 h (empty symbols) solar cells based on: (i) ZnO (red), (ii) AZO<sub>0.03</sub> (black), (iii) AZO<sub>0.37</sub> (blue), and (iv) AZO<sub>0.8</sub> (green) ETL. The plots are relative to devices in which the ZnO-based ETLs are processed in inert atmosphere, N<sub>2</sub> (a), or in air (b). The black arrows highlight the transition of the  $J$ – $V$  curves when passing from fresh to degraded devices.

**Light-Soaking Stability of OPV Devices.** We investigated the light-soaking degradation of polymer solar cells prepared by using the four different formulations of ZnO or AZO<sub>x</sub> NPs (see [Experimental Section](#)). A set of inverted BHJ devices ([Figure 2a](#)) was fabricated using a new polymer P(1) (P(1)-PFQ2T-BDT, [Figure 2b](#)) as donor material. Further details for the synthesis and optical and electrochemical properties of the donor P(1) are reported in the [Supporting Information](#).

Note that all OPV parameters reported and discussed in this section are averaged over 10 samples, based on two identical batches of ZnO/AZO<sub>x</sub> NPs, thus guaranteeing the reproducibility and reliability of the results.

We first investigated the influence of the different ZnO-based ETLs on the photovoltaic response of freshly fabricated devices. The thickness of the ZnO/AZO<sub>x</sub> layers was intentionally fixed around 40 nm in order to avoid limitations arising from the different electrical conductivity of doped and undoped NPs. The ZnO/AZO<sub>x</sub> layers were processed by spin coating in air or in an inert atmosphere (N<sub>2</sub> environment) and successively thermal annealed at 140 °C for 15 min to remove the water content probably adsorbed on the ZnO/AZO<sub>x</sub> structure. Note that, in the case of air processing, after the thermal treatment the films were immediately transferred inside a glovebox to avoid moisture contact.

**Table 2. Photovoltaic Parameters of Degraded Solar Cells (40 h under 1 sun), Based on (i) ZnO, (ii) AZO<sub>0.03</sub>, (iii) AZO<sub>0.37</sub>, and (iv) AZO<sub>0.8</sub> ETLs, Processed Either in Air or in an Inert Atmosphere, N<sub>2</sub><sup>a</sup>**

	ETL	ETL process environment	$J_{sc}$ (mA/cm <sup>2</sup> )	$V_{oc}$ (V)	FF (%)	PCE (%)	$R_s$ ( $\Omega$ cm <sup>2</sup> ) <sup>b</sup>	$R_{sh}$ ( $\Omega$ cm <sup>2</sup> ) <sup>c</sup>
Device A	ZnO	N <sub>2</sub>	7.2 ± 0.3	0.81 ± 0.005	43 ± 1	2.5 ± 0.1	18.6 ± 0.1	310 ± 10
		air	7.5 ± 0.1	0.66 ± 0.002	35 ± 1	1.7 ± 0.1	37.7 ± 0.1	190 ± 10
Device B	AZO <sub>0.03</sub>	N <sub>2</sub>	6.9 ± 0.5	0.81 ± 0.004	46 ± 1	2.6 ± 0.2	16.5 ± 0.1	390 ± 10
		air	7.3 ± 0.3	0.81 ± 0.005	43 ± 1	2.5 ± 0.1	17.1 ± 0.1	320 ± 10
Device C	AZO <sub>0.37</sub>	N <sub>2</sub>	7.0 ± 0.2	0.81 ± 0.007	43 ± 1	2.4 ± 0.1	19.6 ± 0.1	330 ± 10
		air	6.9 ± 0.2	0.72 ± 0.005	40 ± 1	2.0 ± 0.1	20.5 ± 0.1	270 ± 10
Device D	AZO <sub>0.8</sub>	N <sub>2</sub>	6.9 ± 0.3	0.82 ± 0.005	45 ± 1	2.5 ± 0.1	19.5 ± 0.1	380 ± 10
		air	6.8 ± 0.1	0.72 ± 0.005	41 ± 1	2.0 ± 0.1	22.4 ± 0.1	280 ± 10

<sup>a</sup>All the OPV parameters are averaged over 10 samples, and mean values are reported with their standard deviation. <sup>b</sup> $R_s$  was calculated as the slope of the tangent line of the current density–voltage ( $J$ – $V$ ) curve at  $V > V_{oc}$ . <sup>c</sup> $R_{sh}$  was calculated as the slope of the tangent line of the  $J$ – $V$  curve at  $V = 0$ .

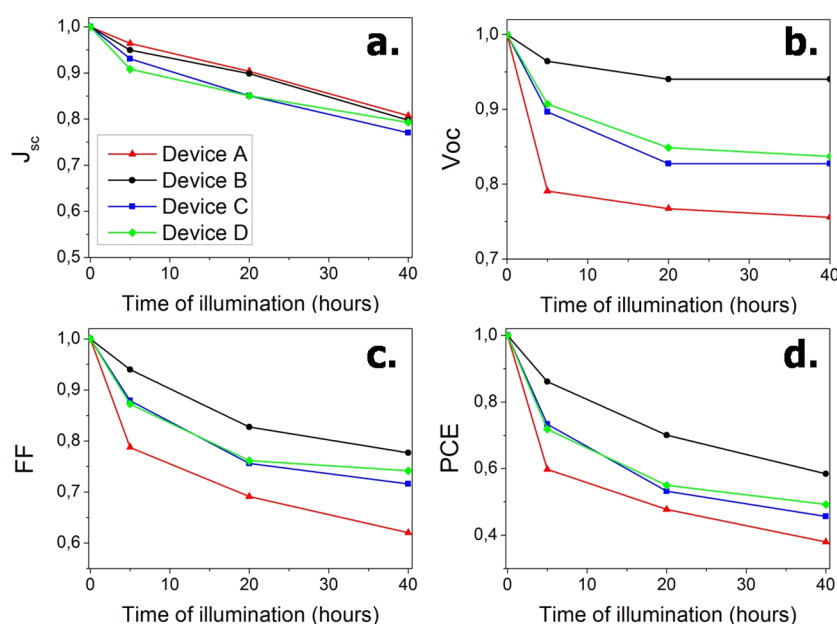


**Figure 4.** Evolution of normalized  $J_{sc}$  (a),  $V_{oc}$  (b), FF (c), and PCE (d) values versus degradation time of devices A, B, C, and D, respectively, based on air-processed ETLs: ZnO (red triangles), AZO<sub>0.03</sub> (black circles), AZO<sub>0.37</sub> (blue squares), and AZO<sub>0.8</sub> (green rhomboids). The devices were degraded under AM1.5G simulated sunlight for 40 h in inert atmosphere.

The OPV parameters of the resulting solar cells are summarized in Table 1. Devices A, B, C, and D show nearly identical photovoltaic performance, with initial PCEs over 4%,  $J_{sc}$  of  $\sim 8.7$  mA/cm<sup>2</sup>,  $V_{oc}$  of  $\sim 0.87$  V, FF of  $\sim 55\%$ , and series ( $R_s$ ) and shunt resistance ( $R_{sh}$ ) of  $\sim 11$  and  $\sim 680$   $\Omega$  cm<sup>2</sup>, respectively. Therefore, the OPV parameters of fresh devices are not affected by the Al doping level in the ZnO layer. This can be expected since the ZnO, AZO<sub>0.03</sub>, AZO<sub>0.37</sub>, and AZO<sub>0.8</sub>-based films show similar optical transmittance, surface roughness, and energy band positions (Figure 1). It should be also noted that the photovoltaic response of the solar cells is independent of the processing environment since it is unvaried if ZnO or AZO<sub>x</sub> films are processed either in inert atmosphere or in air.

In order to investigate the effect of light soaking on the stability of the studied solar cells, all devices were kept in a glovebox under AM1.5G illumination for 40 h, and their current density–voltage ( $J$ – $V$ ) characteristics were measured at defined time intervals.

Figure 3a shows the  $J$ – $V$  plots of fresh and degraded devices A, B, C, and D with the ZnO-based ETLs processed in an inert atmosphere. As mentioned above, all devices exhibit the same initial OPV properties.

After light soaking, the  $J$ – $V$  curves were slightly changed in a similar way for all devices. Indeed, the devices were equally degraded reaching similar OPV parameters (Table 2):  $J_{sc}$  drops to about 7 mA/cm<sup>2</sup>,  $V_{oc}$  to 0.81 V, and FF to 45%, and the PCE decreases from about 4% to 2.5%. A partial decrease of the photovoltaic performance with light soaking can be expected for all devices since BHJ solar cells are commonly affected by at least a partial degradation under prolonged irradiation. Indeed, light catalyzes processes such as for instance photobleaching and morphological changes in the active layer, ion migration from electrodes, trap generation, etc.<sup>36</sup> In most cases, degradation mechanisms are complex and include a variety of processes that can be interlinked. It is therefore very difficult to associate the degradation to a specific layer of the device. However, since the OPV parameters of all the degraded ZnO-based solar cells are comparable, we can assume that the light-induced processes occurring in devices A, B, C, and D are not influenced by the nature of the ZnO-based ETLs (ZnO, AZO<sub>0.03</sub>, AZO<sub>0.37</sub>, or AZO<sub>0.8</sub>) when processed in an inert atmosphere. On the contrary, the degradation trend observed for the devices based on air-processed ETLs is considerably different.

As shown in Figure 3b and Table 2, degraded devices A, B, C, and D based on air-processed ETLs exhibit different  $J$ - $V$  plots. In particular, we found that (i) device A, containing undoped ZnO NPs as ETL, is the less stable; (ii) device B, based on AZO<sub>0.03</sub> NPs (with lowest concentration of aluminum) as ETL, is the most stable; and (iii) devices C–D using AZO NPs with a higher concentration of aluminum (0.37% and 0.8%, respectively) are less stable compared to device B but still show an enhanced photostability with respect to device A. Interestingly, the degraded device B gives the same photovoltaic response (identical  $J$ - $V$  curve) irrespective of the AZO<sub>0.03</sub> processing atmosphere. On the contrary, devices A, C, and D were found to be less stable if the ETLs are deposited in air rather than in inert atmosphere. This indicates that ZnO, AZO<sub>0.37</sub>, and AZO<sub>0.8</sub> layers are affected by light soaking depending on their processing environment, while the AZO<sub>0.03</sub> layer shows an environment-independent behavior in light-soaking degradation. To identify the possible causes of the difference in stability of the ZnO and AZO<sub>x</sub> layers, the trend of decay of the OPV parameters during light exposure was analyzed (Figure 4).

As shown in Figure 4a, the  $J_{sc}$  decreases with a similar linear trend for all air-processed devices. This decrease could be ascribed to degradation mechanisms common to all devices that equally affect the active layer or the active layer/interlayer interfaces since all the cells show the same behavior. Diversely, the decrease of  $V_{oc}$  (Figure 4b), FF (Figure 4c), and PCE (Figure 4d) is considerably different within the four devices, being smaller for the AZO<sub>0.03</sub>-based solar cell. The degradation trend of  $V_{oc}$  and FF for devices A, C, and D is characterized by an initial sharper drop after 5 h of illumination, followed by a smoother decrease up to 40 h. Interestingly, the differences among the degradation trends of the devices are observed only within the first few hours; then,  $V_{oc}$  and FF decrease in the same gradual way for all the cells. Since the solar cells differ only for the nature of their ETLs, the differences in the overall light-soaking stability of devices A, B, C, and D with ETLs processed in air can be likely ascribed to a light-induced and air-dependent degradation process occurring in the first few hours. Moreover, as the decrease of  $V_{oc}$  and FF shows the same trend for all devices, it is reasonable to suppose that their decay is related to the same degradation process. Similar solar cells (with ZnO/AZO<sub>x</sub> films processed in air) have been fabricated using a different active layer based on a polythieno[3,4-*b*]-thiophene-*co*-benzodithiophene (PTB7):PCBM blend. All devices were characterized and then kept under illumination in an inert atmosphere for 24 h. As shown in Figure S4, PTB7-based solar cells showed a degradation behavior similar to that of P(1):PCBM-based solar cells (Figure 4). Indeed, cells using AZO<sub>0.03</sub> film were more stable under prolonged illumination than devices using AZO<sub>0.8</sub> or AZO<sub>0.37</sub> film, and ZnO-based cells were the most affected devices. In addition, the degradation trends are similar to those exhibited by P(1)-based devices confirming that ZnO and AZO<sub>x</sub> films processed in air play an important role in terms of light stability of the resulting devices. However, as all PTB7-based solar cells were highly affected by light-induced degradation after a few hours of illumination (Figure S4),<sup>37</sup> systematic and more detailed investigations have been carried out on P(1)-based devices.

The degradation processes, which involve the ETL of a solar cell, usually affect the bulk conductivity and/or its charge selectivity. When the ETL bulk conductivity decreases during degradation, an increase of the series resistance of the resulting

device is expected. On the contrary, when the charge selectivity of the ETL is reduced, the overall shunt resistance of the device is decreased due to higher charge recombination at the electrodes. As a result, both limitations negatively affect the FF; however, only in the second case small variations of the ETL charge selectivity induce significant changes of FF and  $V_{oc}$  simultaneously.<sup>38</sup> Taking into account these considerations, we compared the series ( $R_s$ ) and shunt ( $R_{sh}$ ) resistances of fresh and degraded air-processed devices A, B, C, and D (Tables 1 and 2). In detail, a slight increase in  $R_s$  is observed after light exposure for all solar cells, with only degraded device A showing a high  $R_s$  (37.7  $\Omega$  cm<sup>2</sup>) if compared to the other ones ( $\sim$ 20  $\Omega$  cm<sup>2</sup>). On the other hand,  $R_{sh}$  is considerably different within degraded devices A, B, C, and D (Table 2). In particular,  $R_{sh}$  is less affected by light soaking for the air-processed ETL prepared with ZnO doped with the lowest aluminum concentration (AZO<sub>0.03</sub>). Contrarily,  $R_{sh}$  of devices based on air-processed ZnO, AZO<sub>0.37</sub>, and AZO<sub>0.8</sub> strongly decreases after light soaking, indicating a reduction in the charge selectivity of the ETLs that consequently affects the  $V_{oc}$  of the corresponding BHJ cells.<sup>39</sup> To further analyze the electrical properties and behavior of the devices, dark  $J$ - $V$  curves of fresh and degraded devices A, B, C, and D, based on air-processed ETLs are reported in Figure 5.

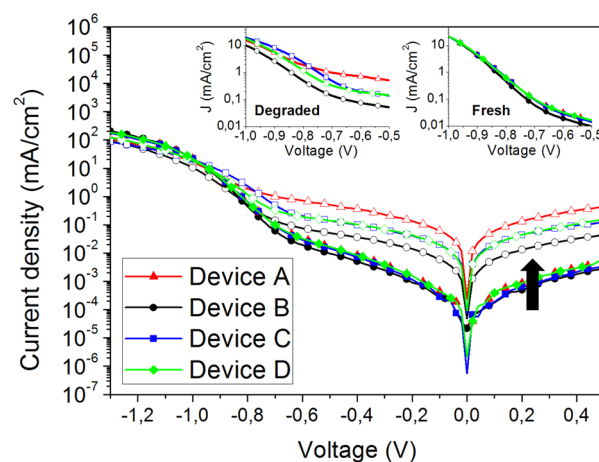


**Figure 5.** Dark  $J$ - $V$  plots (semilogarithmic) of fresh (filled symbols) and degraded under AM1.5G simulated sunlight for 40 h (empty symbols) devices A, B, C, and D, respectively, based on air-processed ZnO (red triangles), AZO<sub>0.03</sub> (black circles), AZO<sub>0.37</sub> (blue squares), and AZO<sub>0.8</sub> (green rhomboids) ETLs. The black arrow highlights the transition of the  $J$ - $V$  curves from fresh to degraded devices. In the insets, a zoom-in of the range between  $-1.0$  and  $-0.5$  V is shown for fresh (right) and degraded (left) devices.

For all degraded devices, the dark  $J$ - $V$  curves in the  $+0.5$  to  $-0.4$  V voltage range show the characteristics of an ohmic resistor. The highest dark current in reverse bias is measured for device A; intermediate values are measured for devices C and D; while the lowest current is measured for device B. This means that the diode behavior of the cells based on AZO<sub>0.37</sub>, AZO<sub>0.8</sub>, and especially for undoped ZnO is poorer than that of the cell based on AZO<sub>0.03</sub>. In addition, by observing the graph in the forward bias region (ranging from  $-0.4$  to  $-1.3$  V), the small slope of the  $J$ - $V$  curve of degraded devices A, C, and D, between  $-0.5$  and  $-1.0$  V (Figure 5 insets), reflects a diode ideality number greater than 1.<sup>39</sup> This behavior in forward bias is indicative of a nonideal recombination of injected charges

due to the presence of shunts in the ETLs, in agreement with the lower  $R_{sh}$  values reported in Table 2.

It has been demonstrated that organic solar cells containing a ZnO film, which has been previously UV soaked in dry air, suffer shunting losses.<sup>40</sup> Indeed, during illumination, the UV treatment of oxygen present in dry air causes the introduction of interstitial oxygen atoms in the ZnO lattice, which act as *p*-type defects.<sup>41,42</sup> As a result, the Fermi level of ZnO decreases, promoting the extraction of holes from the HOMO level of the donor material and consequently rising dark currents in reverse bias.<sup>40</sup> That results in a smaller  $V_{oc}$  in agreement with our observations in the case of devices A, C, and D. Therefore, it is reasonable to assume that oxygen chemisorption on the ZnO/AZO<sub>x</sub> surface during air processing causes the degradation of  $V_{oc}$  and FF under illumination, via formation of shunts as above-mentioned. In addition, since oxygen is present in the ZnO/AZO<sub>x</sub> film in a limited amount, the related degradation process of ETL is evident only in a fixed time interval (a few hours of light soaking). This could explain the fast reduction of FF and  $V_{oc}$  of devices A, C, and D in the first hours. Moreover, the formation of shunt points also explains the simultaneous degradation trend of FF and  $V_{oc}$ .

To verify the occurrence of the UV/oxygen-related degradation process in our systems, all the devices with air-processed ETLs were degraded under UV-filtered AM1.5G simulated sunlight (see Experimental Section). Since oxygen can degrade ZnO/AZO<sub>x</sub> films only under UV irradiation, the use of a filter should hinder the described shunting process. For this reason we measured the  $J$ - $V$  plot of all devices before and after degradation with UV-filtered light.

Figure 6 shows that all the solar cells are now characterized by the same  $J$ - $V$  plot after UV-filtered light-soaking. Device A,

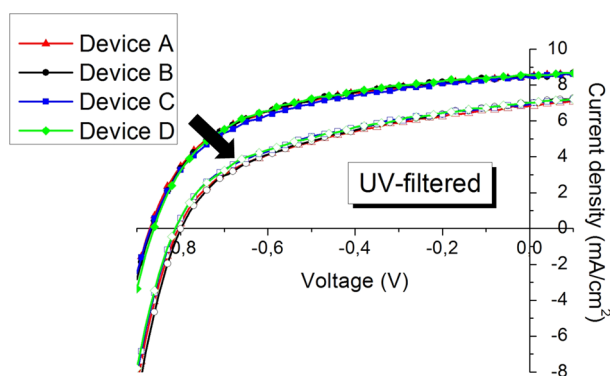


**Figure 6.** Current density–voltage ( $J$ - $V$ ) plot of: (i) ZnO- (red), (ii) AZO<sub>0.03</sub>- (black), (iii) AZO<sub>0.37</sub>- (blue), and (iv) AZO<sub>0.8</sub>- (green) based solar cells before (filled symbols) and after (empty symbols) degradation under UV-cut AM1.5G simulated sunlight for 40 h. All the ZnO-based ETLs are processed in air. The black arrow highlights the transition of the  $J$ - $V$  curves from fresh to degraded devices.

which during normal light-soaking degradation was subjected to substantial photovoltaic losses (Figure 3b), under UV-filtered light-soaking, matches the photovoltaic response of degraded device B, showing a similar stability.

This suggests that, as oxygen cannot interact with the ZnO/AZO<sub>x</sub> NPs, all devices are equally affected by the same degradation processes, which is in this case independent of the ETL nature and is reasonably ascribed to light-induced degradation of the active layer. Accordingly, we recently demonstrated that BHJ devices based on a series of similar

donor polymers are characterized, under prolonged illumination, by photobleaching of the active film which affects the device stability.<sup>43</sup>

We proved that the different behavior of ZnO, AZO<sub>0.03</sub>, AZO<sub>0.37</sub>, and AZO<sub>0.8</sub> ETLs under prolonged illumination is due to the interaction of ZnO/AZO<sub>x</sub> with oxygen, and a clear correlation with the Al doping level in ZnO was also demonstrated. Interestingly, the loss in the photovoltaic performance of air-processed ZnO-based devices after light degradation can be fully recovered by doping ZnO only with a small amount of aluminum (0.03%), while using higher Al doping concentrations restores the oxygen-related light soaking instability of undoped ZnO. To note, even though photo-degradation still occurs for higher Al doping concentrations, the stability of AZO<sub>0.37</sub>- and AZO<sub>0.8</sub>-based devices is improved in comparison to the analogous device based on undoped ZnO.

The origin of the improved photostability for Al-doped ZnO ETLs compared to pristine ZnO may be ascribed to several reasons. First, it was shown recently that the presence of a very thin Al layer between the air-processed ZnO ETL and the active blend can prevent  $V_{oc}$  losses under light-soaking conditions.<sup>39</sup> Indeed, doping the ZnO surface through Al deposition shifts the Fermi level toward the ZnO conducting band, increasing the photostability of the resulting devices. In our case, the doping of the ZnO NPs occurs during synthesis leading to a strong increase in the conductivity of the ETLs as well as passivation of defect states, as evidenced by the reduced intensity of the emission spectra in the visible range.<sup>35,44</sup> Furthermore, it is likely that Al dopants modify the surface chemistry of the ZnO leading to a reduced amount of adsorbed oxygen molecules inside the ETL during air processing. Indeed, oxygen chemisorbs on ZnO structural point defects, in particular Zn vacancies.<sup>29</sup> Aluminum can fill in Zn vacancies, as Al<sup>3+</sup> ions have larger nuclear charge but a smaller atomic radius than Zn<sup>2+</sup>. It appears therefore reasonable to suppose that the number of Zn vacancies is decreased by doping ZnO with aluminum, leading to a reduced amount of adsorbed oxygen inside air-processed ETLs.<sup>35,45–47</sup> Thus, both effects of Al incorporation into the ZnO NPs may contribute to the improved photostability of the corresponding air-processed BHJ cells. However, it is still unclear why devices based on ETLs with higher Al-doping levels (AZO<sub>0.37</sub> and AZO<sub>0.8</sub>) are less photostable than those based on AZO<sub>0.03</sub>. One possibility could be that at higher doping levels aluminum species able to interact with the oxygen are generated at the AZO surface, likely inducing new defect states under prolonged UV exposure. This may lead to transport barriers probably responsible for increased charge recombination processes in the AZO<sub>0.37</sub>- and AZO<sub>0.8</sub>-based devices.

Interestingly, although AZO<sub>0.03</sub> NPs have only a small Al doping level, the electrical conductivity of the resulting film is increased by 3 orders of magnitude compared to the analogous undoped ZnO layer, making it suitable for thick film processing.<sup>35,30</sup> This confirms that AZO NPs, in particular AZO<sub>0.03</sub>, represent an excellent charge-selective material for roll-to-roll processing because, aside from the good electrical conductivity, they lead to clear improvements in the UV stability of air-processed organic solar cells.

## CONCLUSIONS

In summary, we investigated the light-soaking stability under prolonged illumination (40 h under 1 sun) of inverted polymer solar cells based on four different formulations of ZnO NPs

used as ETLs: ZnO, AZO<sub>0.03</sub>, AZO<sub>0.37</sub>, and AZO<sub>0.8</sub>. The ZnO/AZO-based formulations were deposited from solution and processed in two different environments, air or inert atmosphere. We found that, when the ZnO/AZO layers are processed in inert atmosphere, the degradation of the relative solar cells is independent from the grade of Al doping in the NPs. Indeed, all the cells equally degrade after the light soaking test. Diversely, air-processed ZnO/AZO layers differently influence the stability of the relative cells. In particular, ZnO-based devices are the most unstable, while the AZO<sub>0.03</sub>-based cells are the most stable with a degradation behavior which is not affected by the processing environment. Chemisorption of oxygen on ZnO during air processing of the ETL was demonstrated to be the cause of the reduced light-soaking stability of the relative solar cells. In the case of AZO-based ETLs, oxygen chemisorption is suggested to be reduced due to passivation of Zn defect states, improving the stability of the resulting devices under prolonged illumination.

In conclusion, solution-processed AZO NPs, in particular those with low Al doping content, are promising materials for their application as charge-selective layers in the industrial production of air-processed organic solar cells, due to their higher conductivity (required for thick films) and to their higher stability under UV-light prolonged irradiation.

## ■ ASSOCIATED CONTENT

### Supporting Information

The Supporting Information is available free of charge on the ACS Publications website at DOI: 10.1021/acsami.5b08255.

HR-TEM image of AZO<sub>0.03</sub>, synthesis procedure for P(1) polymer, square-wave voltammogram, absorption spectra of P(1) polymer, and  $V_{oc}$  trend over illumination time of PTB7-based solar cells with air-processed ETLs (PDF)

## ■ AUTHOR INFORMATION

### Corresponding Authors

\*E-mail: mirko.seri@isof.cnr.it.

\*E-mail: ackermann@cinam.univ-mrs.fr.

### Author Contributions

All authors have given approval to the final version of the manuscript.

### Notes

The authors declare no competing financial interest.

## ■ ACKNOWLEDGMENTS

This work was supported by FP7 European collaborative project SUNFLOWER (FP7-ICT-2011-7-contract no. 287594). We also acknowledge Laboratory MIST E-R within the *Programma Operativo FESR 2007-2013* of Regione Emilia-Romagna (no. attività I.1.1) and the French *Fond Unique Interministériel* (FUI) under the project "SFUMATO" (Grant number: F1110019 V/201308815) for financial support. In addition, the authors wish to thank Prof. Mats Fahlman for his scientific contribution, Vincenzo Ragona, and Federico Prescimone for the technical support.

## ■ REFERENCES

(1) Dou, L.; You, J.; Hong, Z.; Xu, Z.; Li, G.; Street, R. a.; Yang, Y. 25th Anniversary Article: A Decade of Organic/Polymeric Photovoltaic Research. *Adv. Mater.* **2013**, *25*, 6642–6671.

(2) Prosa, M.; Sagnella, A.; Posati, T.; Tassarolo, M.; Bolognesi, M.; Cavallini, S.; Toffanin, S.; Benfenati, V.; Seri, M.; Ruani, G.; Muccini, M.; Zamboni, R. Integration of a Silk Fibroin based Film as a Luminescent Down-Shifting Layer in ITO-Free Organic Solar Cells. *RSC Adv.* **2014**, *4*, 44815–44822.

(3) Yu, G.; Gao, J.; Hummelen, J. C.; Wudl, F.; Heeger, A. J. Polymer Photovoltaic Cells: Enhanced Efficiencies via a Network of Internal Donor-Acceptor Heterojunctions. *Science* **1995**, *270*, 1789–1791.

(4) Po, R.; Carbonera, C.; Bernardi, A.; Camaioni, N. The Role of Buffer Layers in Polymer Solar Cells. *Energy Environ. Sci.* **2011**, *4*, 285.

(5) Bolognesi, M.; Tassarolo, M.; Posati, T.; Nocchetti, M.; Benfenati, V.; Seri, M.; Ruani, G.; Muccini, M. Efficiency Enhancement of P3HT:PCBM Solar Cells Containing Scattering Zn-Al Hydroxalite Nanoparticles in the PEDOT:PSS Layer. *Org. Photonics Photovoltaics* **2013**, *1*, 1–10.

(6) Yusoff, A. R. B. M.; Kim, D.; Kim, H. P.; Shneider, F. K.; da Silva, W. J.; Jang, J. A High Efficiency Solution Processed Polymer Inverted Triple-Junction Solar Cell Exhibiting a Power Conversion Efficiency of 11.83%. *Energy Environ. Sci.* **2015**, *8*, 303–316.

(7) Hösel, M.; Søndergaard, R. R.; Jørgensen, M.; Krebs, F. C. Failure Modes and Fast Repair Procedures in High Voltage Organic Solar Cell Installations. *Adv. Energy Mater.* **2014**, *4*, 1–7.

(8) Tassarolo, M.; Guerrero, A.; Gedefaw, D.; Bolognesi, M.; Prosa, M.; Xu, X.; Mansour, M.; Wang, E.; Seri, M.; Andersson, M. R.; Muccini, M.; Garcia-Belmonte, G. Predicting Thermal Stability of Organic Solar Cells Through an Easy and Fast Capacitance Measurement. *Sol. Energy Mater. Sol. Cells* **2015**, *141*, 240–247.

(9) He, Z.; Zhong, C.; Su, S.; Xu, M.; Wu, H.; Cao, Y. Enhanced Power-Conversion Efficiency in Polymer Solar Cells Using an Inverted Device Structure. *Nat. Photonics* **2012**, *6*, 593–597.

(10) Hau, S. K.; Yip, H.-L.; Baek, N. S.; Zou, J.; O'Malley, K.; Jen, A. K. Y. Air-Stable Inverted Flexible Polymer Solar Cells Using Zinc Oxide Nanoparticles as an Electron Selective Layer. *Appl. Phys. Lett.* **2008**, *92*, 253301.

(11) Sachs-Quintana, I. T.; Heumüller, T.; Mateker, W. R.; Orozco, D. E.; Checharoen, R.; Sweetnam, S.; Brabec, C. J.; McGehee, M. D. Electron Barrier Formation at the Organic-Back Contact Interface is the First Step in Thermal Degradation of Polymer Solar Cells. *Adv. Funct. Mater.* **2014**, *24*, 3978–3985.

(12) Li, Z.; Chiu, K. H.; Ashraf, R. S.; Fearn, S.; Dattani, R.; Wong, H. C.; Tan, C. H.; Wu, J.; Cabral, J. T.; Durrant, J. R. Toward Improved Lifetimes of Organic Solar Cells under Thermal Stress: Substrate-Dependent Morphological Stability of PCDTBT:PCBM Films and Devices. *Sci. Rep.* **2015**, *5*, 15149.

(13) Clark, M. D.; Jespersen, M. L.; Patel, R. J.; Leever, B. J. Predicting Vertical Phase Segregation in Polymer-Fullerene Bulk Heterojunction Solar Cells by Free Energy Analysis. *ACS Appl. Mater. Interfaces* **2013**, *5*, 4799–4807.

(14) Guerrero, A.; Pfannmöller, M.; Kovalenko, A.; Ripolles, T. S.; Heidari, H.; Bals, S.; Kaufmann, L.; Bisquert, J.; Garcia-belmonte, G. Nanoscale Mapping by Electron Energy-Loss Spectroscopy Reveals Evolution of Organic Solar Cells Contact Selectivity. *Org. Electron.* **2015**, *16*, 227–233.

(15) Sun, Y.; Seo, J. H.; Takacs, C. J.; Seifert, J.; Heeger, A. J. Inverted Polymer Solar Cells Integrated with a Low Temperature-Annealed Sol-Gel-Derived ZnO Film as an Electron Transport Layer. *Adv. Mater.* **2011**, *23*, 1679–1683.

(16) Liang, Z. Q.; Zhang, Q. F.; Wiranwetchayan, O.; Xi, J. T.; Yang, Z.; Park, K.; Li, C. D.; Cao, G. Z. Effects of the Morphology of a ZnO Buffer Layer on the Photovoltaic Performance of Inverted Polymer Solar Cells. *Adv. Funct. Mater.* **2012**, *22*, 2194–2201.

(17) Woo, S.; Kim, W. H.; Kim, H.; Yi, Y.; Lyu, H. K.; Kim, Y. 8.9% Single-Stack Inverted Polymer Solar Cells with Electron-Rich Polymer Nanolayer-Modified Inorganic Electron-Collecting Buffer Layers. *Adv. Energy Mater.* **2014**, *4*, 1301692.

(18) Gilot, J.; Barbu, I.; Wienk, M. M.; Janssen, R. A. J. The use of ZnO as optical spacer in polymer solar cells: Theoretical and experimental study. *Appl. Phys. Lett.* **2007**, *91*, 113520.

- (19) Dkhil, S. B.; Duché, D.; Gaceur, M.; Thakur, A. K.; Aboura, F. B.; Escoubas, L.; Simon, J. J.; Guerrero, A.; Bisquert, J.; Garcia-Belmonte, G.; Bao, Q.; Fahlman, M.; Vidolot-Ackermann, C.; Margeat, O.; Ackermann, J. Interplay of Optical, Morphological, and Electronic Effects of ZnO Optical Spacers in Highly Efficient Polymer Solar Cells. *Adv. Energy Mater.* **2014**, *4*, 1400805.
- (20) Jeon, I.; Ryan, J. W.; Nakazaki, T.; Yeo, K. S.; Negishi, Y.; Matsuo, Y. Air-Processed Inverted Organic Solar Cells Utilizing a 2-Aminoethanol-Stabilized ZnO Nanoparticle Electron Transport Layer that Requires No Thermal Annealing. *J. Mater. Chem. A* **2014**, *2*, 18754–18760.
- (21) Morfa, A. J.; Macdonald, B. I.; Subbiah, J.; Jasieniak, J. J. Understanding the Chemical Origin of Improved Thin-Film Device Performance from Photodoped ZnO Nanoparticles. *Sol. Energy Mater. Sol. Cells* **2014**, *124*, 211–216.
- (22) Jin, Y.; Wang, J.; Sun, B.; Blakesley, J. C.; Greenham, N. C. Solution-Processed Ultraviolet Photodetectors Based on Colloidal ZnO Nanoparticles. *Nano Lett.* **2008**, *8*, 1649–1653.
- (23) Manor, A.; Katz, E. a.; Tromholt, T.; Krebs, F. C. Electrical and Photo-Induced Degradation of ZnO Layers in Organic Photovoltaics. *Adv. Energy Mater.* **2011**, *1*, 836–843.
- (24) Trost, S.; Zilberberg, K.; Behrendt, A.; Polywka, A.; Görm, P.; Reckers, P.; Maibach, J.; Mayer, T.; Riedl, T. Overcoming the “Light-Soaking” Issue in Inverted Organic Solar Cells by the Use of Al:ZnO Electron Extraction Layers. *Adv. Energy Mater.* **2013**, *3*, 1437–1444.
- (25) Bai, S.; Jin, Y.; Liang, X.; Ye, Z.; Wu, Z.; Sun, B.; Ma, Z.; Tang, Z.; Wang, J.; Würfel, U.; Gao, F.; Zhang, F. Ethanedithiol Treatment of Solution-Processed ZnO Thin Films: Controlling the Intragap States of Electron Transporting Interlayers for Efficient and Stable Inverted Organic Photovoltaics. *Adv. Energy Mater.* **2015**, *5*, 1401606.
- (26) MacLeod, B. a.; Tremolet de Villers, B. J.; Schulz, P.; Ndione, P. F.; Kim, H.; Giordano, A. J.; Zhu, K.; Marder, S. R.; Graham, S.; Berry, J. J.; Kahn, A.; Olson, D. C. Stability of Inverted Organic Solar Cells with ZnO Contact Layers Deposited from Precursor Solutions. *Energy Environ. Sci.* **2015**, *8*, 592–601.
- (27) Romero-Gomez, P.; Betancur, R.; Martinez-Otero, A.; Elias, X.; Mariano, M.; Romero, B.; Arredondo, B.; Vergaz, R.; Martorell, J. Enhanced Stability in Semi-Transparent PTB7/PC71BM Photovoltaic Cells. *Sol. Energy Mater. Sol. Cells* **2015**, *137*, 44–49.
- (28) Liu, H.; Wu, Z.; Hu, J.; Song, Q.; Wu, B.; Lam Tam, H.; Yang, Q.; Choi, W. H.; Zhu, F. Efficient and Ultraviolet Durable Inverted Organic Solar Cells Based on an Aluminum-Doped Zinc Oxide Transparent Cathode. *Appl. Phys. Lett.* **2013**, *103*, 043309.
- (29) Wilken, S.; Parisi, J.; Borchert, H. Role of Oxygen Adsorption in Nanocrystalline ZnO Interfacial Layers for Polymer-Fullerene Bulk Heterojunction Solar Cells. *J. Phys. Chem. C* **2014**, *118*, 19672–19682.
- (30) Stubhan, T.; Oh, H.; Pinna, L.; Krantz, J.; Litzov, I.; Brabec, C. J. Inverted Organic Solar Cells Using a Solution Processed Aluminum-Doped Zinc Oxide Buffer Layer. *Org. Electron.* **2011**, *12*, 1539–1543.
- (31) Park, S.; Tark, S. J.; Lee, J. S.; Lim, H.; Kim, D. Effect of Intrinsic ZnO Buffer Layer Based on P3HT/PCBM Organic Solar Cells with Al-Doped ZnO Electrode. *Sol. Energy Mater. Sol. Cells* **2009**, *93*, 1020–1023.
- (32) Jagadamma, L. K.; Al-Senani, M.; El-Labban, A.; Gereige, I.; Ngongang Ndjawa, G. O.; Faria, J. C. D.; Kim, T.; Zhao, K.; Cruciani, F.; Anjum, D. H.; McLachlan, M. a.; Beaujuge, P. M.; Amassian, A. Polymer Solar Cells with Efficiency > 10% Enabled via a Facile Solution-Processed Al-Doped ZnO Electron Transporting Layer. *Adv. Energy Mater.* **2015**, *5*, 1500204.
- (33) Oh, H.; Krantz, J.; Litzov, I.; Stubhan, T.; Pinna, L.; Brabec, C. J. Comparison of Various Sol-Gel Derived Metal Oxide Layers for Inverted Organic Solar Cells. *Sol. Energy Mater. Sol. Cells* **2011**, *95*, 2194–2199.
- (34) Stubhan, T.; Litzov, I.; Li, N.; Salinas, M.; Steidl, M.; Sauer, G.; Forberich, K.; Matt, G. J.; Halik, M.; Brabec, C. J. Overcoming Interface Losses in Organic Solar Cells by Applying Low Temperature, Solution Processed Aluminum-Doped Zinc Oxide Electron Extraction Layers. *J. Mater. Chem. A* **2013**, *1*, 6004–6009.
- (35) Gaceur, M.; Dkhil, S. B.; Duché, D.; Simon, J. J.; Escoubas, L.; Dachraoui, W.; Diallo, K.; Guerrero, A.; Mansour, M.; Belmonte, G. G.; Liu, X.; Fahlman, M.; Vidolot-Ackermann, C.; Margeat, O.; Ackermann, J.; et al. Ligand-free synthesis of Aluminum doped Zinc Oxide nanocrystals and their use as optical spacers in color tuned high-efficient organic solar cells. *Adv. Funct. Mater.* **2015**, n/a DOI: 10.1002/adfm.201502929.
- (36) Jørgensen, M.; Norrman, K.; Krebs, F. C. Stability/Degradation of Polymer Solar Cells. *Sol. Energy Mater. Sol. Cells* **2008**, *92*, 686–714.
- (37) Lim, F. J.; Krishnamoorthy, A.; Ho, G. W. Device Stability and Light-Soaking Characteristics of High-Efficiency Benzodithiophene-Thienothiophene Copolymer-Based Inverted Organic Solar Cells with F-TiO<sub>x</sub> Electron-Transport Layer. *ACS Appl. Mater. Interfaces* **2015**, *7*, 12119–12127.
- (38) Servaites, J. D.; Ratner, M. A.; Marks, T. J. Organic Solar Cells: A New Look at Traditional Models. *Energy Environ. Sci.* **2011**, *4*, 4410–4422.
- (39) Kam, Z.; Wang, X.; Zhang, J.; Wu, J. Elimination of Burn-In Open-Circuit Voltage Degradation by ZnO Surface Modification in Organic Solar Cells. *ACS Appl. Mater. Interfaces* **2015**, *7*, 1608–1615.
- (40) Bao, Q.; Liu, X.; Xia, Y.; Gao, F.; Kauffmann, L. D.; Margeat, O.; Ackermann, J.; Fahlman, M. Effect of Ultraviolet Soaking on Surface Electronic Structures of Solution Processed ZnO Nanoparticle Films in Polymer Solar Cells. *J. Mater. Chem. A* **2014**, *2*, 17676–17682.
- (41) Adhikary, P.; Venkatesan, S.; Adhikari, N.; Maharjan, P. P.; Adebajo, O.; Chen, J.; Qiao, Q. Enhanced Charge Transport and Photovoltaic Performance of PBDTTT-C-T/PC<sub>70</sub>BM Solar Cells Via UV-Ozone Treatment. *Nanoscale* **2013**, *5*, 10007–10013.
- (42) Cho, J. M.; Kwak, S. W.; Aqoma, H.; Kim, J. W.; Shin, W. S.; Moon, S. J.; Jang, S. Y.; Jo, J. Effects of Ultraviolet-Ozone Treatment on Organic-Stabilized ZnO Nanoparticle-Based Electron Transporting Layers in Inverted Polymer Solar Cells. *Org. Electron.* **2014**, *15*, 1942–1950.
- (43) Gedefaw, D.; Tessarolo, M.; Prosa, M.; Bolognesi, M.; Henriksson, P.; Zhuang, W.; Seri, M.; Muccini, M.; Andersson, M. R. Induced Photodegradation of Quinoxaline Based Copolymers for Photovoltaic Applications. *Sol. Energy Mater. Sol. Cells* **2016**, *144*, 150–158.
- (44) Wei, W.; Zhang, C.; Chen, D.; Wang, Z.; Zhu, C.; Zhang, J.; Lu, X.; Hao, Y. Efficient “Light-soaking”-free Inverted Organic Solar Cells with Aqueous Solution Processed Low-Temperature ZnO Electron Extraction Layers. *ACS Appl. Mater. Interfaces* **2013**, *5*, 13318–13324.
- (45) Aprilia, A.; Wulandari, P.; Suendo, V.; Herman; Hidayat, R.; Fujii, A.; Ozaki, M. Influences of Dopant Concentration in Sol-Gel Derived AZO Layer on the Performance of P3HT:PCBM Based Inverted Solar Cell. *Sol. Energy Mater. Sol. Cells* **2013**, *111*, 181–188.
- (46) Kuo, S. Y.; Chen, W. C.; Lai, F. I.; Cheng, C. P.; Kuo, H. C.; Wang, S. C.; Hsieh, W. F. Effects of Doping Concentration and Annealing Temperature on Properties of Highly-Oriented Al-Doped ZnO Films. *J. Cryst. Growth* **2006**, *287*, 78–84.
- (47) Pachoumi, O.; Li, C.; Vaynzof, Y.; Banger, K. K.; Sirringhaus, H. Improved Performance and Stability of Inverted Organic Solar Cells with Sol-Gel Processed, Amorphous Mixed Metal Oxide Electron Extraction Layers Comprising Alkaline Earth Metals. *Adv. Energy Mater.* **2013**, *3*, 1428–1436.